

Numerical investigation of the buckling behavior of thin ferrocement stiffened plates

Apostolos Koukouselis* and Euripidis Mistakidis^a

Laboratory of Structural Analysis and Design, Department of Civil Engineering, University of Thessaly, Pedion Areos, GR-38334 Volos, Greece

(Received July 10, 2013, Revised December 5, 2014, Accepted December 27, 2014)

Abstract. One of the most common applications of ferrocement is the manufacturing of thin stiffened plates which are prone to buckling. This study focuses on the investigation of the behavior of a ferrocement plate, stiffened in both directions by means of an appropriate grid of ribs. In the present paper detailed three-dimensional numerical Finite Element models are formulated for the simulation of the behavior of the structure under study, which are able to take into account both the geometric and material non-linearities that are present in the subject at hand (plasticity, cracking, large displacements). The difference among the formulated models lies on the use of different types of finite elements. The numerical results obtained by each model are compared and the most efficient model is determined. Finally, this model is in the sequel used for the further investigation of the effect of different parameters on the ultimate load capacity, such as the initial out-of-plane imperfection of the plate and the interaction between the axial loads in both directions.

Keywords: computational mechanics; construction materials; ferrocement; finite elements method; non-linear analysis

1. Introduction

As Naaman (2000) describes, ferrocement is a form of reinforced concrete, widely used in the construction of thin-walled sections, consisting of closely spaced multiple layers of mesh and/or small diameter rods, usually made of steel and a hydraulic cement mortar. Fig. 1 demonstrates a typical ferrocement structural element. Although there are many similarities between ferrocement and reinforced concrete (R/C) and the general guidelines and standards regarding R/C structures also apply to ferrocement ones, the distinct differences in their behavior should be taken into account during the analysis and design of such elements. In contrast to R/C, ferrocement elements have reinforcement distributed throughout their thickness in both directions with typical reinforcement ratios that are a lot higher than those of conventionally reinforced elements (2-8% total or 1-4% in each direction). These facts lead to elements which have:

- (a) high tensile strength (of the same order as the compressive one),

*Corresponding author, Ph.D. Student, E-mail: akoukouselis@gmail.com

^aProfessor, E-mail: emistaki@uth.gr

- (b) high ductility that, unlike in R/C elements, increases with the increase of the reinforcement ratio,
- (c) homogeneous-isotropic properties in two directions, and
- (d) high punching shear resistance.

Also, due to the fact that the reinforcement comes in the form of thin wire-meshes and not of thick rods, the cracking, and thus the bending behavior, is different from that of R/C. Similarly to fiber-reinforced concrete elements, the cracking stage (stage II) can be quite extensive, sometimes even until the yielding of the mesh (no stage III). Moreover, the crack width and spacing observed in ferrocement is one order of magnitude smaller than that of R/C. That leads to excellent durability (Naaman 2000).

Over the years, extensive research has taken place in the area of buckling of stiffened steel or aluminium plates, especially by engineers in the field of marine and offshore structures. The high compressive and tensile ultimate stress of structural steel and aluminium lead engineers into the construction of structures of small thickness which, however, are sensitive to buckling. Ferrocement, as a high performance composite material, also finds application in such lightweight structures of small thickness but little research has been performed concerning the buckling behavior of ferrocement stiffened plates. Although the same analysis and design principles also apply in ferrocement stiffened plates, certain parameters, such as cracking, may differentiate their behavior with respect to that of steel structures and needs to be taken under consideration.

In the analysis of stiffened plates, as mentioned in the relevant literature (Ventsel and Krauthammer (2001); Tvergaard V. (1973); Stamatelos *et al.* (2011); Paik *et al.* (2008)), three cases may appear regarding buckling (Fig. 2):

- (a) Global buckling modes, which are dominant in the case that the plate is rather thick.
- (b) Local buckling modes of the plate between the stiffeners. These modes are dominant in cases of thin plates under the presence of strong stiffeners.
- (c) Mixed buckling modes. These modes arise in case of thin plates stiffened by relatively weak stiffeners.

Important parameters in the behavior of stiffened plates are:

- The geometry and spacing of the stiffeners;
- The aspect ratio of the plates between the stiffeners;
- The thickness of the plate;
- The boundary conditions.

As mentioned above, the boundary conditions at the edges of the structural elements have a significant influence on the buckling and post-buckling behavior of the structure. Another important parameter in the behavior of stiffened plates that may cause a reduction of the ultimate load-capacity is the initial out-of-plane imperfection of the plate. Significant interaction between the modes may occur and thus stiffened plates are considered very “imperfection sensitive”. Out of mode initial imperfections may even lead to an increase of the ultimate strength (Amdahl (2009)). As a result, the strength of perfect plates, easily calculated by analytical methods, can and should be used as an important reference, however geometrically and materially nonlinear analyses with different possible initial imperfections have to be performed by the use of effective methods such as the FEM (Ueda *et al.* (1995)).

In this paper a slender ferrocement structure is studied. Due to the small thickness of the structure, the buckling response governs the structural behavior. In addition to the geometrical non-linearities, material non-linearities are expected to have a great effect on the overall resistance of the structure, as is the case with all reinforced concrete structures. Due to the lack of detailed

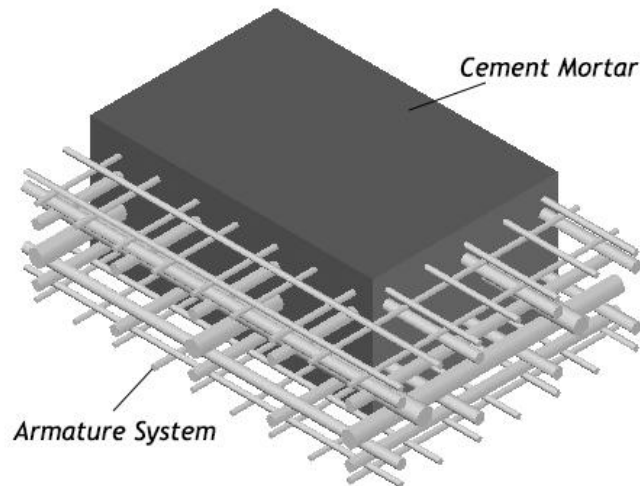


Fig. 1 Typical ferrocement cross section

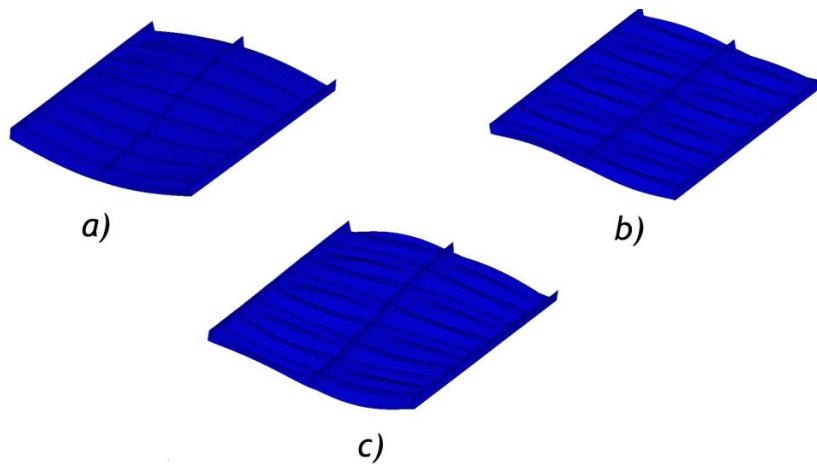


Fig. 2 Typical buckling modes of stiffened plates a) Global buckling mode, b) Local buckling mode, c) Mixed buckling mode

analysis and design recommendations in the Eurocode parts related to the design of concrete or cementitious structures (Eurocode 2 (2005)), methodologies followed in the design of steel structures are applied here (Eurocode 3-Part 1.6 (2007)). The structure is studied following the fully numerical calculation procedure referenced as “Design by global numerical analysis using GMNIA analysis” (GMNIA: Geometrical and Material Nonlinear analysis of the Imperfect shell).

Section 2 describes the considered structural problem, while Section 3 summarizes the applied modeling methodologies. In Section 4 the paper deals with the elastic stability analysis of two stiffened plates with thicknesses of 20 mm and 35 mm respectively. The main scopes are first to determine the preliminary buckling mode in both directions and, if possible, reduce the size of the model and second to investigate the interaction between the axial loads in each direction.

Moreover, different methods of simulation are studied and compared.

In Section 5, the simulation method used in order to appropriately take into account the material nonlinearity of ferrocement is discussed and the results of the nonlinear analysis of the stiffened plate are presented. The effect of the magnitude of the initial imperfections and the presence of axial load in the transverse direction are investigated and discussed.

2. The structure under investigation

The structure under investigation is a stiffened in both directions plate, under in plane loads. The structure consists of a repeating 5×5 m unit, whose geometry is shown in Fig. 3. It consists of a ferrocement skin of small thickness, stiffened in both directions by a grid of ribs. In the x direction the spacing of the 250 mm deep ribs (ribs- x) is 2500 mm, while parallel to the y axis there is a 200 mm deep rib (rib- y) every 625 mm. Both ribs- x and ribs- y are 45 mm thick. The out-of-plane displacement (u_z) of the stiffened plate is restrained by lines of point supports in a pattern which is shown in Fig. 3. The distance between point supports in each line of support is 5m while a line of support exists every 2.5 m. The materials used in the structure at hand are cementitious mortar C60 and reinforcing mesh of grade B500c.

In order to investigate the effect of the thickness of the plate on the ultimate buckling load two cases are studied, with subpanel-plate thicknesses of 20 mm and 35 mm respectively. The loading conditions investigated are axial compression in each direction separately, as well as simultaneous axial compression in both directions.

As far as the reinforcement is concerned, in the case of the 20 mm thick subpanel plate, it consists of three types of mesh (# \emptyset 0.8/6.25 mm, # \emptyset 1.6/12.5 mm and # \emptyset 2.5/25 mm) and two types of rods (\emptyset 8 and \emptyset 12). Fig. 4 shows the different reinforcing patterns of the ribs. The reinforcement ratio is about 5% in each direction. As mentioned above, although very similar to common reinforced concrete, the high reinforcement ratio, the small diameter of the rods and their distribution are expected to differentiate the behavior of the material, bringing it closer to the ductile and homogeneous behavior of steel.

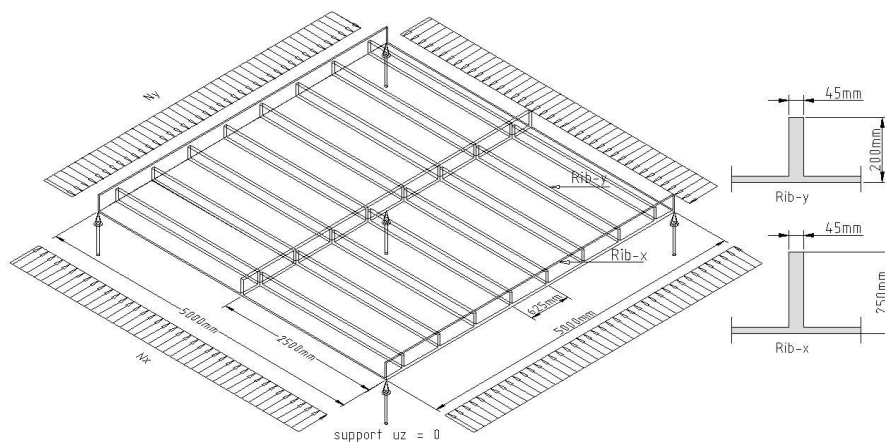


Fig. 3 Geometry of the repeating 5×5 m unit

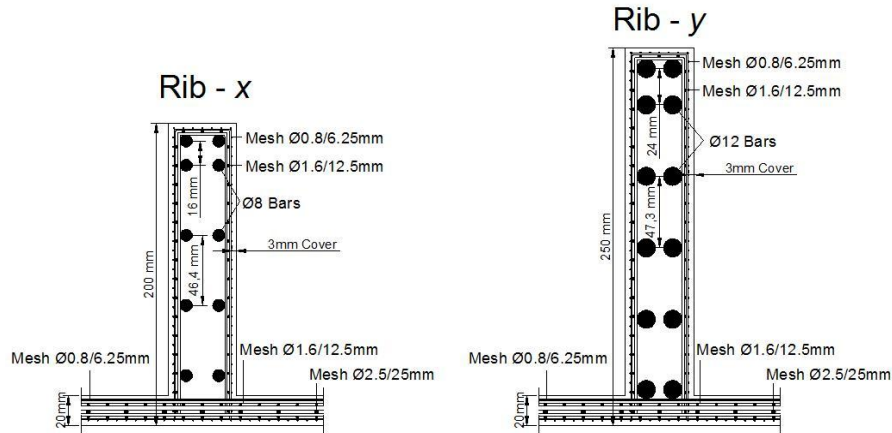


Fig. 4 Reinforcing patterns for the grid of ribs and the 20 mm thick plate

3. Numerical simulation methods

For the buckling analysis of the structure three models were formulated with the MSC-Marc F.E. analysis software (MSC Marc 2011). The first one utilized 4-node thick shell elements (Fig. 5). The shell elements representing the plate had a thickness of 20 or 35 mm, depending on the case investigated, while the shells simulating the grid of ribs were 45 mm thick. The load was applied uniformly along the edges of the finite elements, both on the skin and on the ribs, with its value depending on the thickness of the shell element, so that no eccentricity arises.

The second model (Fig. 6) simulated the stiffened plate by the use of 8-node solid elements. Both the skin and the grid of ribs and beams had one element in the thickness direction. The axial pressure was applied on the face of the solid elements, again taking care to eliminate any load eccentricities.

The third simulation model that was tested was a hybrid one (Fig. 7), in which the grid of ribs was simulated by the use of 2-node Timoshenko beam elements and the skin by 4-node thick shell elements. The centers of mass of the shell elements were connected with the centers of the ribs-*y* with rigid arms while the real position of the center of the ribs-*x* was defined through an offset of the 2-node beam element (Fig. 8). The properties of the rib sections were calculated by hand and were inserted in the model. A part of the load was applied at the edge of the shell elements, while the rest was applied as point loads at the edge nodes of the beam elements so that the no load eccentricity occurs.

For the nonlinear analyses, presented in Section 5, models completely made of composite layered shell elements were used, as this resulted to be the optimal modeling methodology.

As far as the material properties are concerned, for the buckling analyses all elements were considered to be made of a homogeneous isotropic elastic material with a Young's modulus of 34000 N/mm^2 and a Poisson's ratio of 0.1. For the nonlinear analyses, reinforcing steel was considered to be anisotropic with modulus of elasticity equal to 200000 MPa and stiffness only in the direction of the rods. Its elastic-plastic constitutive law was considered bilinear, with a yield stress of 435 MPa and no hardening (Fig. 9a). As far as the concrete mortar is concerned, it was considered isotropic with an elasticity modulus of 34000 MPa. The mortar had an ultimate

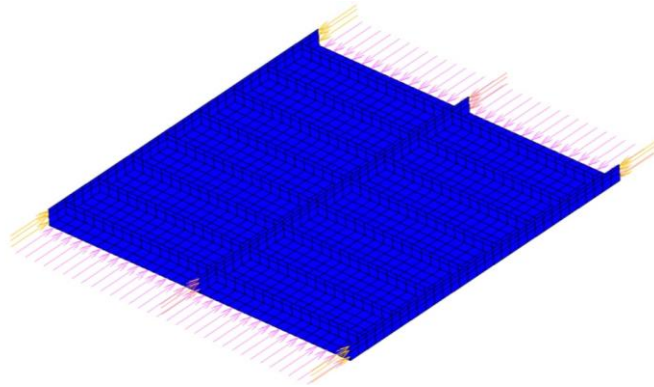


Fig. 5 The 5×5 m shell model and its loading conditions

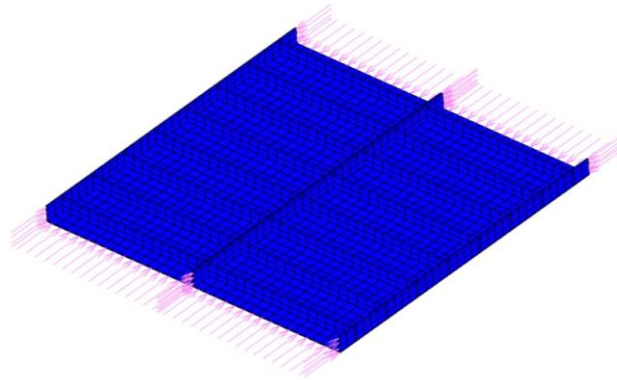


Fig. 6 The 5×5 m solid model and its loading conditions

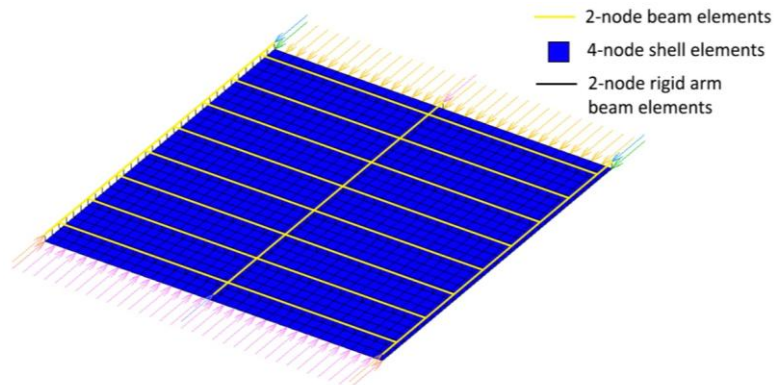


Fig. 7 The 5×5 m hybrid model and its loading conditions

compressive strength of 40 MPa, while cracking was taken under consideration by enabling the damage effect capabilities of MSC Marc. The ultimate tensile stress was considered to be 2 MPa and the softening modulus was equal to 34000 MPa (Fig. 9(b)). The Tresca yield stress criterion was used.

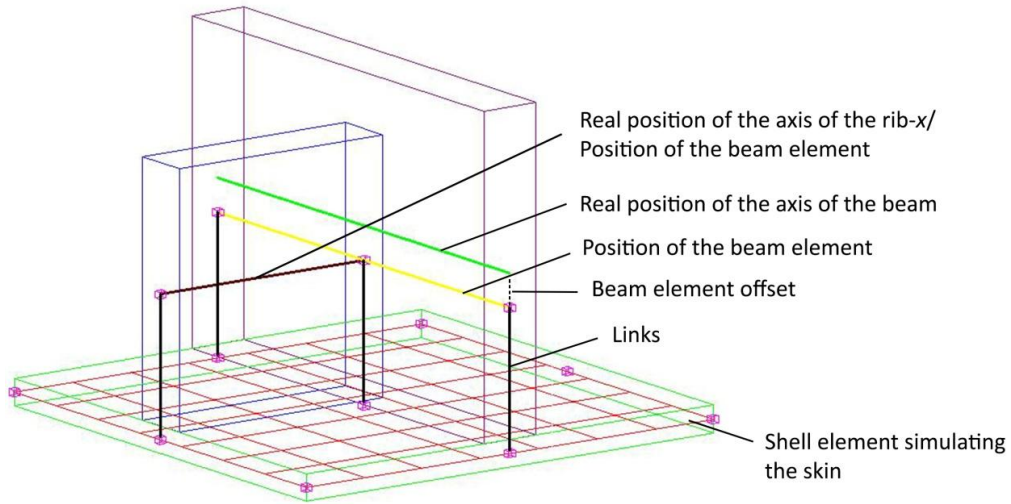


Fig. 8 Hybrid model detail

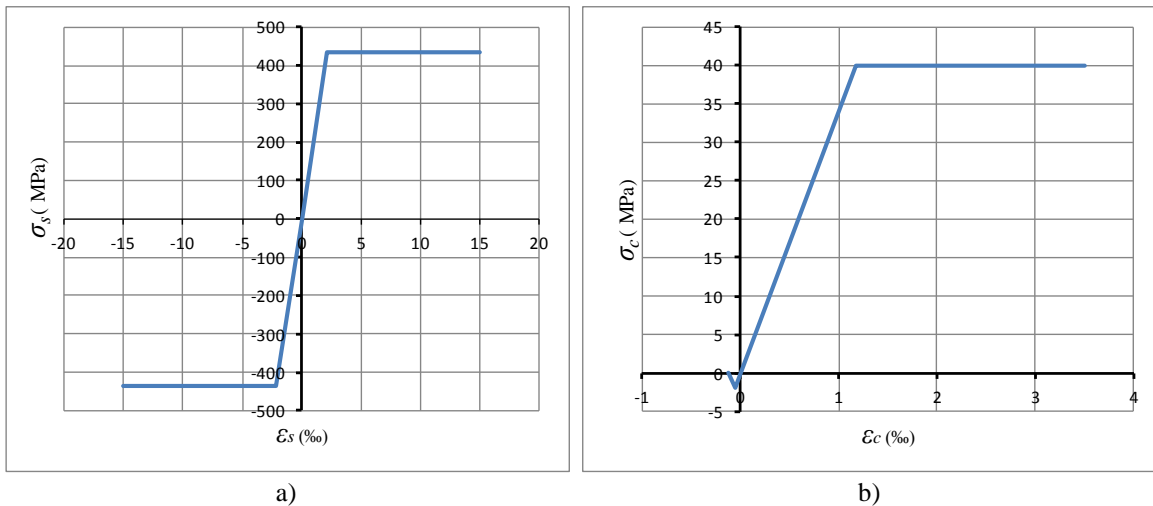


Fig. 9 Constitutive Law for a) the reinforcing steel and b) the cement mortar

The models were solved by an iterative full Newton-Raphson procedure and the convergence criterion was based on the residual forces. The inverse power sweep method was used for the solution of the buckling problem. The nonlinear analysis solution was based on the large strain theory and the full layer integration method was used for the composite layered shells.

4. Modal buckling analysis

The scope of this set of analyses is to determine the fundamental buckle eigenmodes of the ribbed skin in each direction and investigate how they are affected by the thickness of the skin. Moreover, it is also of interest the interaction between the axial loads in the x and y directions. It is

common practice in this type of studies to use periodical boundary conditions in order to reduce the modeled area and study the buckling and post buckling behavior of continuous stiffened plates (Khedmati *et al.* (2009); Mittelstedt (2007); (2009); Fujikubo *et al.* (2006); Byklum *et al.* (2004); Paik and Seo (2009)). Therefore, in the first stage, the boundary conditions that should be applied at the edges of a typical 5×5 m area of the ribbed skin will be determined (symmetry or anti-symmetry boundary conditions).

4.1 Buckling behavior of the 20 mm thick plate

The first simulation models that were tested numerically were formulated through 4-node thick shell elements (Shell Models). The buckling modes in each direction and the boundary conditions that can be applied on a 5x5m region were determined by loading the central 5×5 m region of a 27.5×25 m model and gradually increasing the loaded area. The outer (not loaded) spans simulate

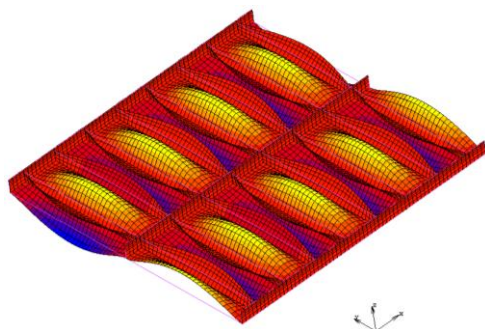


Fig. 10 Buckle mode for loading along the x-axis

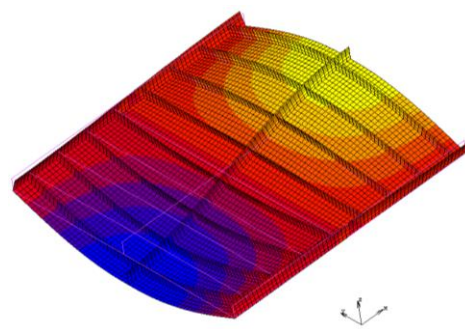


Fig. 11 Buckle mode for loading along the y-axis

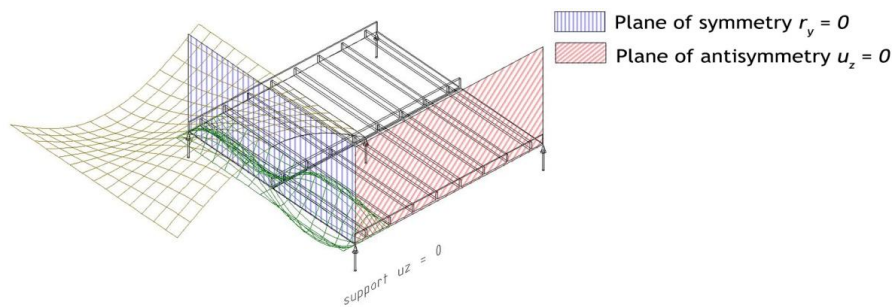


Fig. 12 Boundary conditions of the repeating 5×5 m unit for the 20 mm thick plate

Table 1 Summary and comparison of the calculated buckling loads

Load (kN/m)	Shell Model			3D Model			Hybrid Model		
	156 mm square mesh	78 mm square mesh	39 mm square mesh	156 mm square mesh	78 mm square mesh	39 mm square mesh	156 mm square mesh	78 mm square mesh	39 mm square mesh
N_{bx}	1449	1287	1245	1467	1333	1290	1396	1261	1230
N_{by}	2678	2665	2661	2771	2748	2737	2673	2661	2649

the continuity of the ribbed skin in both directions without imposing any additional boundary conditions that may lead the model to buckle in a certain way which may not be the critical one. In order to prevent a rigid body movement in the x - y plane, the displacement along the x axis of two nodes lying on the yz plane of symmetry and the displacement along the y axis in the x - z plane of symmetry were restrained.

When the central 5×5 m and 15×15 m areas are loaded, the structure buckles in the x and y directions respectively, according to the modes presented in Figs. 10 and 11 respectively. It is evident that the ribbed plate buckles along the x -axis between the stiffeners due to the presence of a 200×45 mm rib every 625 mm, while along the y -axis a global buckling mode develops. In general, these results are in agreement with the usually considered modes in the stability analysis of stiffened plates. Based on these buckling shapes, the boundary conditions shown in Fig. 12 may be applied in the 5×5 m repeating unit, in order to further investigate the buckling behavior of the stiffened plate by significantly reducing the computational cost. Next, three mesh sizes were tested with 156 mm, 78 mm and 39 mm square shell elements respectively, in order to determine the most efficient one. At the same time, as mentioned in Section 3, two more simulation methods were investigated. The first one used 8-node solid elements (3D Model), while the second one considered shell elements for the plate and beam elements for the stiffeners (Hybrid Model). The results presented in Table 1 show that both the shell and the beam-shell models simulate the behavior of the stiffened plate satisfactorily, while a 78 mm mesh is adequate to accurately investigate the buckling behavior of the ribbed plate.

4.2 Buckling Behavior of the 35 mm thick plate

Once again, initially the central 5×5 m region of a 27.5×25 m model was loaded and gradually the loaded area was increased. While along the y -axis the buckling shape remains the same, when loaded along the x -axis the stiffened plate buckles between the lines of support, following a rather sinusoidal shape, as shown in Fig. 13. When the boundary conditions shown in Fig. 14 are applied at the outer edge of a fully loaded 15×15 m model, the buckling mode changes to a global one. This phenomenon is caused mainly due to the fact that in the 27.5×25 m model the outer (not loaded) areas act as rotational springs, adding stiffness to the loaded area, while in the 15×15 m model a global buckling shape develops, in which all spans lose their stability at the same time. As a conclusion from this set of analyses, it is safe to say that the 35 mm thick ribbed skin will buckle globally in both directions with a chessboard-like pattern. Again, the periodic boundaries of the two buckle shapes at the edges of the repeating 5×5 m unit are the same and thus any $n \times 5 \times m \times 5$ model (n, m integers) will have boundary conditions of symmetry along the y edges and antisymmetry along the x edges.

Table 2 Summary and comparison of the calculated buckling loads

Load (kN/m)	Shell Model			3D Model			Hybrid Model		
	156 mm square mesh	78 mm square mesh	39 mm square mesh	156 mm square mesh	78 mm square mesh	39 mm square mesh	156 mm square mesh	78 mm square mesh	39 mm square mesh
N_{bx}	2792	2780	2776	2859	2835	2824	2789	2778	2774
N_{by}	2785	2774	2770	2905	2882	2871	2783	2773	2769

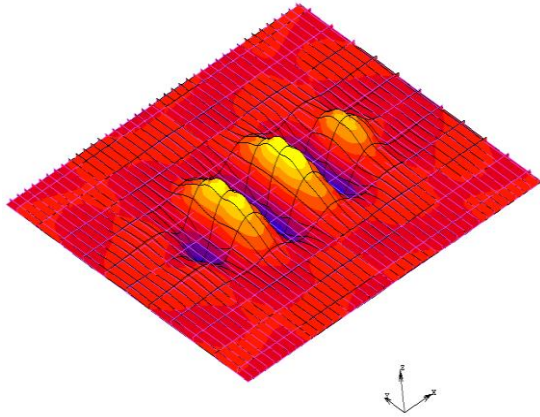


Fig. 13. Buckling shape of the 25×27.5 m model

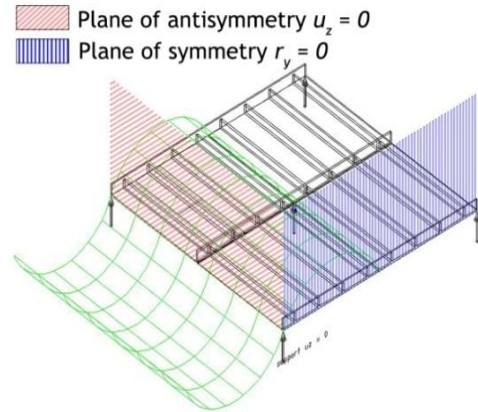


Fig. 14. Boundary conditions of the repeating 5×5 m unit for 35 mm thick plate according to the buckling shape shown in Fig. 13

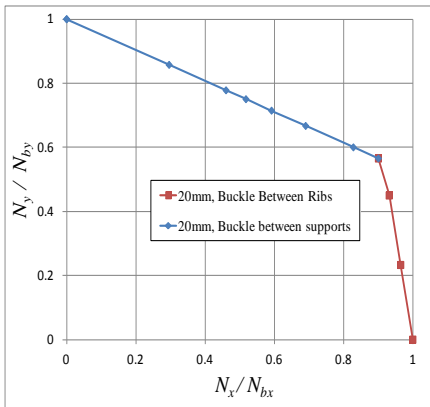


Fig. 15 Interaction diagram for 20 mm thick plate.

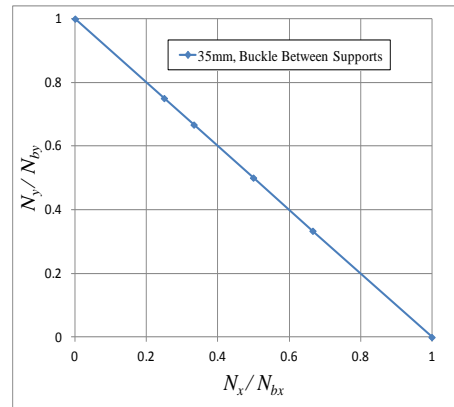


Fig. 16 Interaction diagram for 35 mm thick plate.

In the sequel, different simulation methods and mesh sizing were tested on a 5×5 m model, whose results are presented in Table 2. Again the shell and hybrid shell-beam models seem to be more efficient than the solid one, while even the 156 mm mesh seems to simulate adequately the behavior of the plate.

4.3 Interaction of the axial loads

After investigating the behavior of the stiffened plate for axial compression in each direction separately, and in order to fully comprehend the buckling behavior of the structure, the interaction of the axial loads in the x and y directions is investigated. Similarly to the previous set of analyses, a 5×5 m model is formulated, with boundary conditions corresponding to the dominant buckling shapes and additional out of plane restrains (deflection equals to zero) at the positions of the point supports. The mesh sizing in the x - y plane is 78×78 mm and thick shell elements are used for the

discretization of the problem.

As Figs. 15 and 16 demonstrate, the axial load in the transverse direction reduces the bearing capacity of the ribbed plate. If the ratio of N_x / N_{bx} (applied axial load x - x to buckling load x - x) exceeds the value of 0.9, the buckling resistance in the y direction drops dramatically. This is caused by the change of the buckling mode from buckling between the point supports (global mode) to buckling between ribs (local mode). On the other hand, when the thickness of the plate is increased, both directions buckle under the same axial load between the point supports (global mode) and, therefore, the decrease of the bearing capacity is linear and symmetric as expected.

5. Geometric and material nonlinear analysis of the imperfect plate

5.1 Modeling of the composite material

5.1.1 Modeling of the grid of ribs

Before modeling the entire structure, consisting of the ferrocement skin and the ribs, a single reinforced rib was modeled and tested numerically, in order to verify that its bending behavior is accurately represented. As early as the late 80's (Bergan and Holand (1979)), methods and guidelines for the simulation of R/C elements existed. The most common one is based on the use of shell elements (or plain stress elements in case of 2D problems) to simulate the cement mortar matrix and beam elements to simulate the reinforcing rods and mesh. Although this method accurately simulates the bending behavior with respect to the strong axis of the cross-section, it cannot simulate the bending behavior with respect to the weak axis and the torsional behavior of the rib. In such cases the position of the reinforcement in the thickness directions needs to be accurately simulated. In the case treated here, when the primary buckling is investigated, the bending around the strong axis is dominant, while for buckling between ribs the out-of-plane and torsional behavior of the ribs needs to be accurately simulated. Thus, the method used in this study is based on the use of composite layered shells to simulate the entire reinforced section. The behavior of the rib is studied both under pure bending and under bending with axial force, through a four-point-bending simulation model. The results of the analysis are compared with the ones calculated by the Section Designer module of SAP2000 v15 software (Computers and Structures Inc. 2011) by direct integration of the cross-section. In Table 3 the material properties are summarized, Figs. 17, 18 present the cross section of the composite layered shell, while Fig. 19 shows how these shells are combined to simulate the cross section under investigation.

Table 3 Properties of the materials used in the model

	Behavior	E (GPa)	f_{cd}/f_{yd} (MPa)	f_{ctd} (MPa)
Concrete C60	Isotropic Elastic-perfectly plastic	34	40	2.0 (Cracking with softening modulus 34000 MPa)
Steel B500c	Orthotropic Elastic-perfectly plastic	200 (only in the direction of reinforcement)	435	-

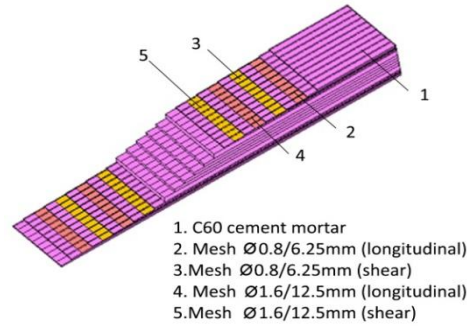
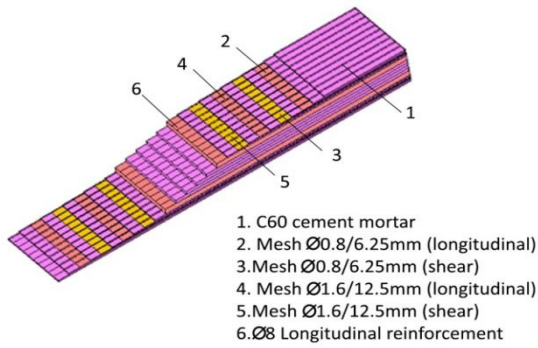


Fig. 17 Composite representing the reinforcement layers

Fig. 18 Composite representing the concrete with mesh reinforcement

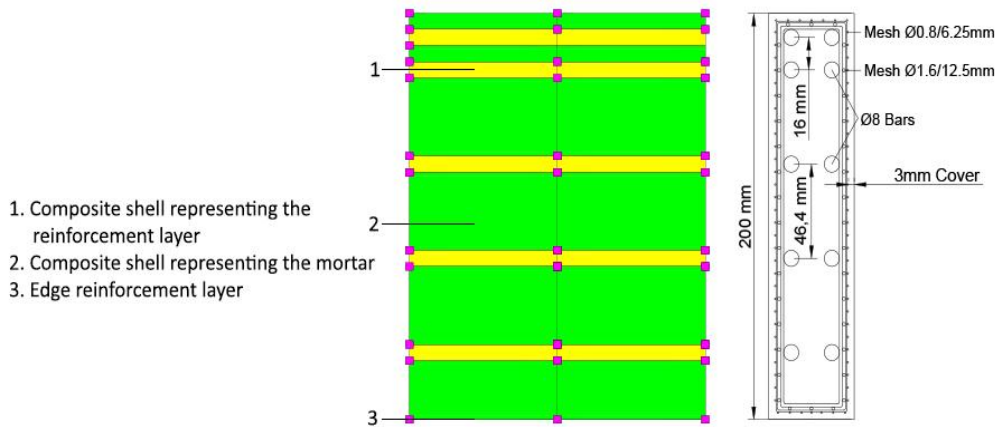


Fig. 19 Simulation of the cross section by the use of the two composite layered shells

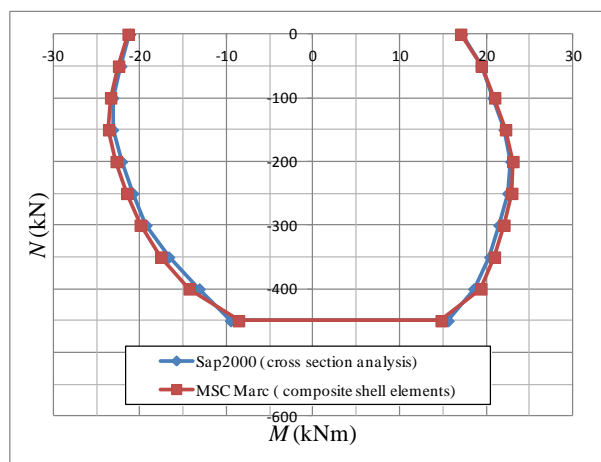


Fig. 20 Comparison of the composite layered shell interaction curve to the one obtained by SAP2000v15

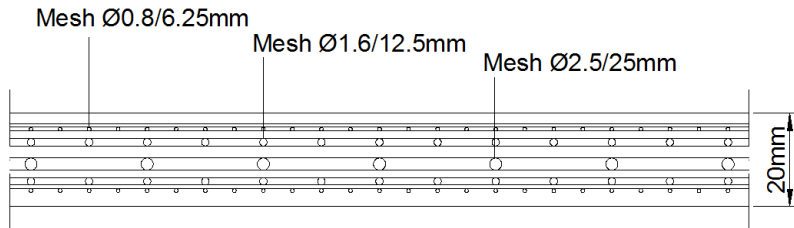


Fig. 21 Cross section of the plate

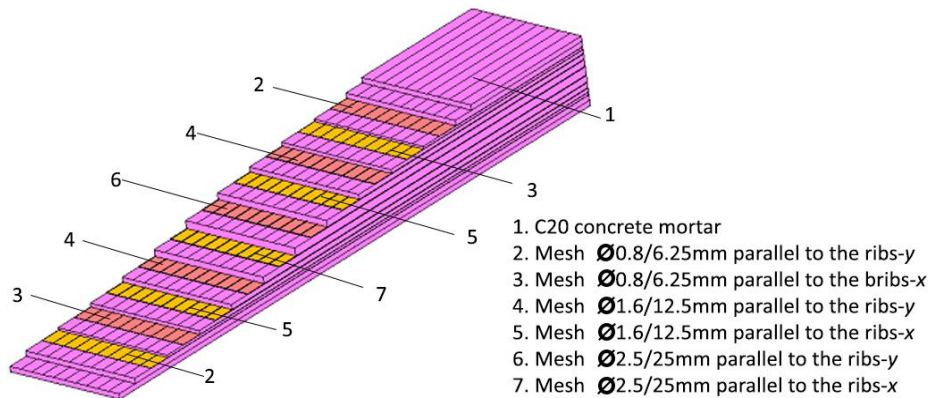


Fig. 22 Composite layered shell element simulating the plate

Fig. 20 demonstrates the comparison of the interaction curve obtained by the use of composite layered shells to the one obtained by direct integration of the cross-section (SAP2000 v15). The comparison shows that the adopted numerical model can accurately simulate the bending behavior of the ferrocement rib.

5.1.2 Modeling of the plate

As with the grid of ribs, before proceeding to a nonlinear finite element analysis, it is necessary to validate the modeling technique regarding the material nonlinearity. As the bending behavior with respect to the weak axis needs to be simulated, the position of the reinforcement in the thickness directions needs to be accurately modelled. Thus, as discussed in Section 5.1.1, the simulation of the cross section by the use of composite layered shells is necessary. The materials used in this set of analyses are identical to the ones used in the modeling of the grid of ribs. Each layer of reinforcement rods was simulated as an equivalent layer of steel. Bond slip effects were not taken into account. The models were solved by an iterative full Newton-Raphson procedure and the convergence criterion was based on the residual forces. Second order effects were not taken into account, as the scope of this investigation is to verify that material nonlinearity is accurately simulated.

The geometry of the shell under study was based on the geometry of the 20 mm thick shell case and is shown in Fig. 21. Fig. 22 demonstrates a graphical representation of the composite shell. The shell was 78.125 mm wide and was subjected to four point bending.

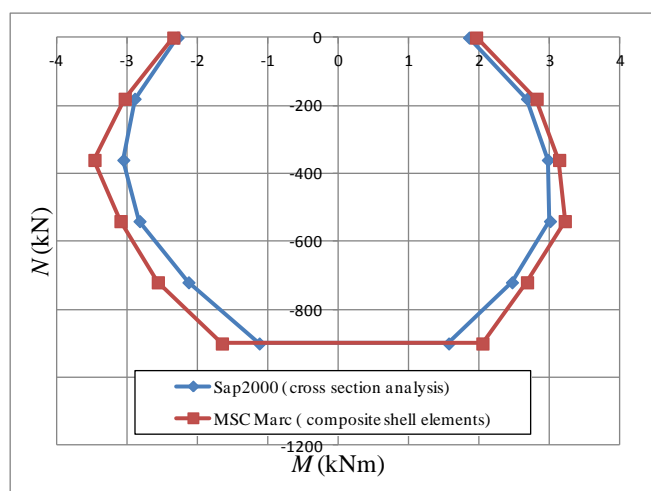


Fig. 23 Comparison of the composite layered shell interaction curve to the one obtained by SAP2000v15

The comparison of the results calculated by integration of the section with the ones produced by the numerical model is shown in Fig. 23. Although the results match rather well when the compressive load is relatively low, a small deviation can be observed for high compressive loads. The main reason for the deviation is that in the MSC-Marc model, after entering the in the plastic regime, transverse compressive stresses appear in the concrete layers, causing the stresses in the main direction to increase. However, the recorded differences are considered insignificant, taking also into account that in the actual model stresses exist in both directions.

5.2 Nonlinear analysis of cases exhibiting global buckling behaviour

The preliminary modal buckle analysis of the 35 mm thick models for both loading directions, as well as the analysis of the 20 mm thick plate for load along the heavily stiffened direction (y axis), showed that the stiffened plate has a relatively high elastic buckling load due to the global buckling mode that develops. A set of nonlinear large strain analyses with initial imperfection in accordance to the global buckling mode and imperfection magnitude equal to 20 mm, confirmed that in these cases the stiffened plate buckles in a global mode with an ultimate load carrying capacity very close to the resistance of the structure in pure compression. As the local buckling parallel to the x axis of the 20 mm thick stiffened plate results in significantly lower resistance, only this case is further investigated.

5.3 Nonlinear analysis of the cases exhibiting local buckling behavior (20 mm thick plate, load parallel to the x -axis)

When both geometric and material nonlinearities are considered, the problem becomes highly complex. Therefore, taking advantage of the symmetry or anti-symmetry of the dominant buckling mode that develops, a 5×5 m model was employed. The properties of the ribs- y that exist at the two edges were adjusted in order to take into account the fact that they should have half the

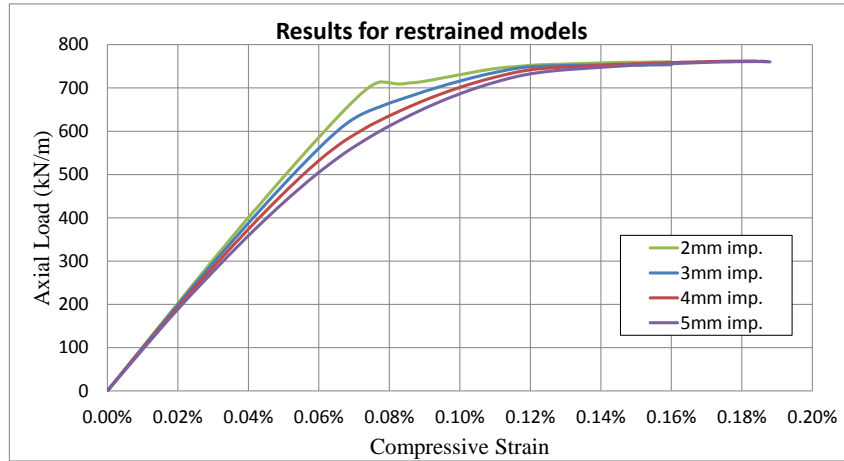


Fig. 24 Response of the 2.5×5 m model for different initial imperfections

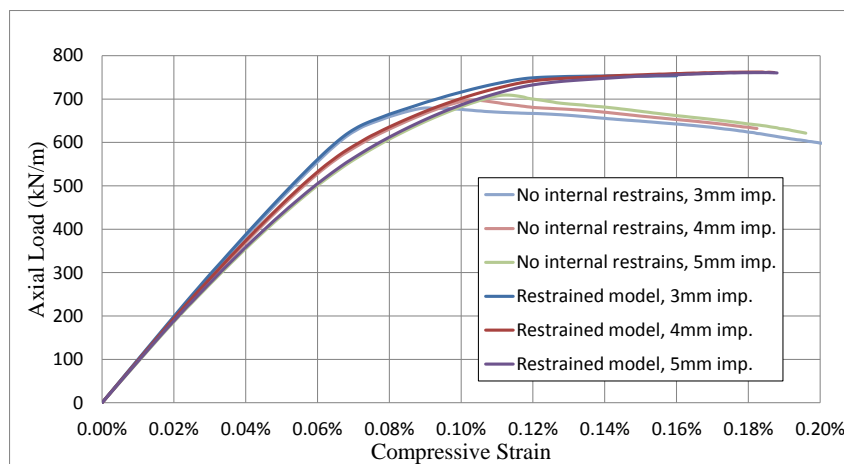


Fig. 25 Comparison of the 5×5 m models with different magnitude of initial imperfection

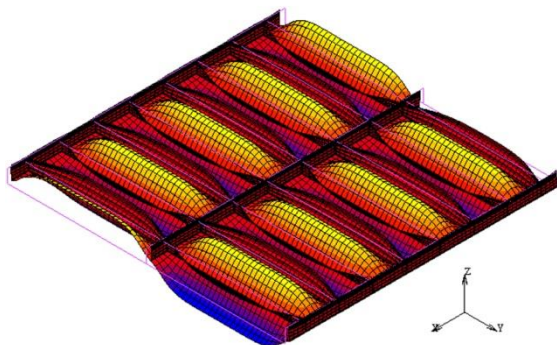


Fig. 26 Failure of the restrained model

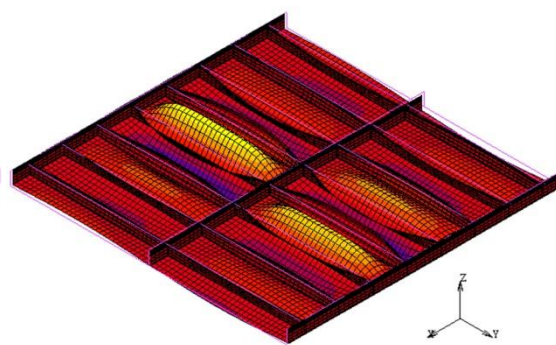


Fig. 27 Failure of the unrestrained model. Localization of failure

Table 4 Calculation and comparison of the γ ratios for loading along the x direction

Thickness of plate	h_{st} (mm)	b_{st} (mm)	I_{st}/b (mm ⁴ /mm)	D (mm ⁴)	γ
20 mm	250	45	23437.5	673.4	34.8
35 mm	250	45	23437.5	3609	6.5

stiffness of the whole rib and half its strength, on the grounds that they are cut by the plane of anti-symmetry. That is achieved by reducing to half the Young's Modulus and the ultimate stresses of the materials for those ribs.

In order to eliminate as possible the instabilities of the model, internal restrains were imposed in each plane where conditions of symmetry or anti-symmetry of the buckling mode arises. In more detail, these restrains impose the in-plane deflections in each plane of anti-symmetry and the in-plane rotations in each plane of symmetry to be equal to zero. In the sequel, these models will be referred to as "restrained" ones. This set of analyses provides an upper bound for the buckling load, corresponding to the simultaneous buckling of all the spans. The analyses included geometrical imperfections, considered to be similar in shape to the dominant buckling mode. The deflections of the buckling mode were scaled accordingly in order to produce results for a family of imperfections having maximum values equal to 2,3,4 and 5 mm.

Fig. 24 presents the results for different initial imperfection magnitudes. It is clear that the increase of the maximum value of the initial imperfections causes a reduction of the stiffness. However, it seems that all models reach their ultimate strength for a similar axial load of about 760 kN/m, although their equilibrium path prior to buckling is different.

To further investigate the buckling behavior of the stiffened plate, all internal restrains were removed and only boundary conditions of symmetry along the x edges and anti-symmetry along the y edges were imposed. Fig. 25 compares the results for the models with internal restrains, considered to be the upper bound of the buckling load, with the results for the "unrestrained" ones. The "unrestrained" models have the same pre-buckle behavior with the restrained ones and lose stability under the slightly lower axial load. The drop of strength, after the maximum load has been attained, is caused by the localization of the buckling failure (Figs. 26 and 27). This phenomenon is caused by the small variations of the imperfection magnitude between spans, as well as by the nonlinearity of the material. As certain spans fail earlier than others, the surrounding areas release their stored strain energy, pushing them further in the plastic region. Also, as the imperfections become larger, the buckling load slightly increases, something that is not surely expected. This is likely caused by the fact that the buckling behavior of stiffened plates can be very sensitive to the used imperfections and small differences between the imperfections used in the various areas can cause differences in the numerically calculated load bearing capacities of the structure. Even in the formulation of a numerical model, such cases cannot be eliminated and are also affected by the intense material non-linearity. However, it is usually neglected during the design of such plates and a lower bound of the buckling load should be used.

5.4 The influence of combined bi-axial compression

Finally, the influence of the axial load in the y direction (N_y) is investigated. The models used in this set of analyses were equipped with internal restrains. Axial loads up to 600 kN/m were applied in the y direction. Fig. 28 demonstrates the results for axial load in the y direction equal to 200, 400 and 600 kN/m, while Fig. 29 presents the interaction curve obtained by this set of analyses,

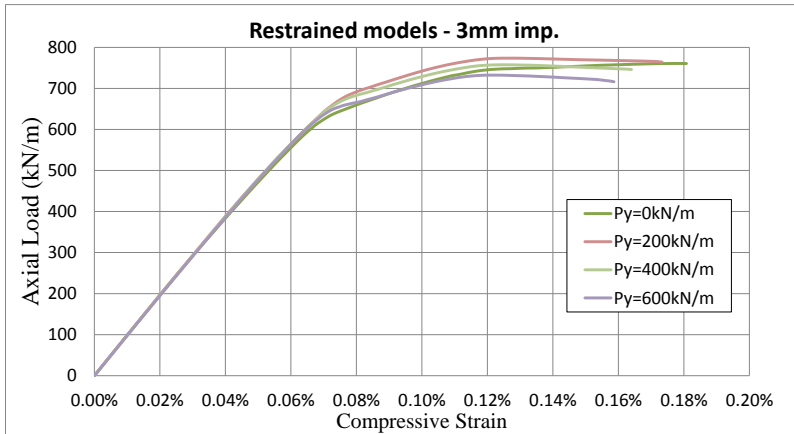


Fig. 28 Influence of axial load in the transverse direction

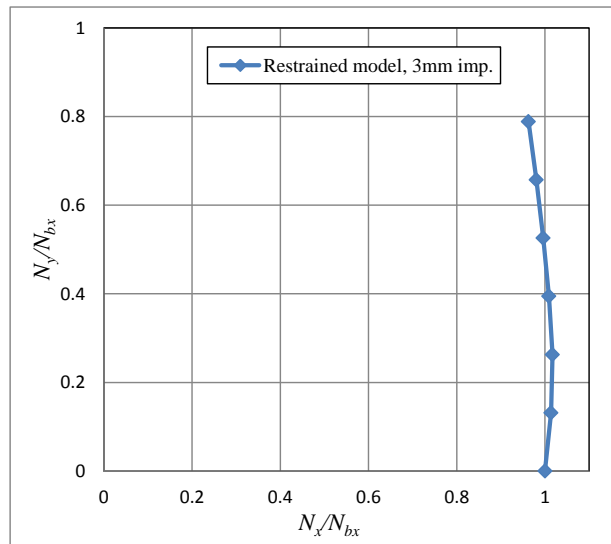


Fig. 29 Interaction curve

which is in agreement with interaction curves found in the literature for similar problems (Byklum *et al.* (2004)). The influence of bi-axial compression seems to be insignificant for the structure at hand. Such behavior is expected from structures non-slender in the y direction, with small aspect ratio of the spans and high length-to-plate thickness ratio.

6. Discussion

Based on the results of the presented buckling analyses it is safe to say that the dominant buckle shapes of the ribbed skin are:

- in the case of the 20 mm thick plate for loading along the x direction, the local buckling of the subpanels with the ribs following their deformation;
- for loading in the y direction of the 20 mm thick stiffened plate and for both loading directions of the 35 mm thick one, the global buckling between the supports.

The main factor that affects the shape of buckling seems to be the thickness of the plate or, more accurately, the ratio of the stiffness of the skin to the stiffness of the supporting ribs. While in the case of the 20 mm thick skin the structure buckles between the ribs along the x axis, when the thickness is increased to 35 mm, the buckling between supports becomes dominant. This type of buckling behavior is common in stiffened steel and aluminum plates as former studies have shown (Paik *et al.* (2008); Mittelstedt (2007, 2009); Fujikubo *et al.* (2006); Byklum *et al.* (2004); Paik and Seo (2009)). Ueda *et al.* (1995) mention, concerning the buckling behavior of longitudinally stiffened plates, that the switch from overall to local buckling is governed by the relative stiffness ratio of the stiffeners to the plate, γ , which is given by the relation:

$$\gamma = EI_{sl} / b' D \quad (1)$$

where I_{sl} is the moment of inertia of the longitudinal stiffeners, b' is the spacing of the stiffeners and $D = (Et^3 / 12(1-\nu^2))$ is the bending resistance of the plate

If γ is smaller than a certain value γ_{\min}^B , then the plate buckles in a global mode while if it is larger, then the subpanels buckle locally. Table 4 presents the calculated γ ratio for loading along the x direction for the two different cases, regarding the thickness of the plate, studied in this paper. It can be noticed that the values of γ between the two cases differ significantly. Hence, the difference in their behavior is justified. The value of γ_{\min}^B depends on the geometry and mechanical properties of the structure as well as on the ratio of the load components in the two transverse directions.

In Table 4, h_{sl} is the height of the stiffeners in the longitudinal direction and b_{sl} is the width of the stiffeners in the longitudinal direction.

Moreover, as the analyses have shown, another important factor governing the buckling behavior of the structure is the applied boundary conditions. These boundary conditions greatly affect the interaction between the global and local buckling modes. The interaction between buckling modes is more profound in the case of the 35mm thick plate where, depending on whether or not the outer span provides rotational support to the inner region, the buckle mode in the x direction switches from a rather sinusoidal shape to a more complex chessboard-like one.

When material and geometrical nonlinearities are taken into account, the problem becomes very complex and it is impossible to be handled with an analytical approach. The numerical design method of EC3 part 1.6 seems to be appropriate for the analysis and design, even for structures that are not made of steel, on the grounds that it is based on general analysis and design principles rather than assumptions that only apply to specific structures. Also, if the structure at hand consists of a basic repeating unit, the modeled area, and thus the computational cost, can be reduced to the one of the basic unit by applying appropriate periodical boundary conditions. These boundary conditions should be carefully chosen according to the critical buckling mode so that they represent the real behavior of the structure.

Moreover, stiffened plates are usually very sensitive to imperfections (Tvergaard (1973)). A deviation from the shape of the critical buckle mode may cause the structure to have a false increase of its ultimate resistance, while small variations of the imperfections between spans may cause localization of the buckling and the failure of the plate for lower axial load, by the buckling

of certain spans. Thus, it is obvious that a set of analyses with different imperfections and boundary conditions should be carried out in order to obtain the lower bound of the buckling load that can be safely used during the design of such structures.

7. Conclusions

An investigation of the buckling behavior of a stiffened ferrocement plate was presented in this study. The fully numerical approach of EC-3 part 1.6 was followed. The analysis procedure consists of:

- Linear buckling analysis (LBA). This set of analyses is used to determine the dominant buckling modes, the shape of the initial imperfections used in the geometrically and materially nonlinear analysis and, finally, the periodic boundary conditions that can be used to reduce the size of the model.
- Geometrically and materially nonlinear analyses of the imperfect plate (GMNIA) to determine the plastic buckling resistance of the structure.

The LBA showed that two buckling modes are critical; global buckling between supports, with half-wave length of 5m, and local buckling of the subpanels between ribs. The main factor that affects the buckling shape is the relative stiffness ratio γ between the stiffeners and the plate. The other important factor is the applied boundary conditions that also control the interaction between modes.

As the results of the GMNIA show, plasticity causes a drop of the buckling resistance by 40%. It is quite obvious that the application of an analytical approach is impossible, as the geometrical and material nonlinearities, together with the effect of the stiffeners, cause high complexity. The numerical approach of the EC-3 part 1.6 seems to be appropriate for the design and analysis of such structures.

As far as the impact of the imperfections is concerned, they seem to have little influence on the ultimate load capacity, however, local buckling is very sensitive to localization and thus small deviations between the magnitudes of the initial imperfections between subpanels may cause the structure to fail before reaching its maximum resistance.

Finally, the influence of bi-axial compression seems not to be dominant for the structure at hand. Based on existing research on similar problems (Ventsel and Krauthammer (2001)), such behavior is expected for structures which are non-slender in one of the two loading directions, with small aspect ratio of the span edges and with high length-to plate thickness ratios.

References

- Computers and Structures, Inc. (2011), "SAP2000 analysis reference manual", *Comput. Struct.*, Inc. Berkeley, California, USA.
- EN1992-1-2 (2005), *Eurocode 2: Design of Concrete Structures - Part 1-1: General Rules and Rules for Buildings*, Brussels.
- EN1993-1-6 (2007), *Eurocode 3: Design of Steel Structures Part 1-6: Strength and Stability of Shell Structures*, Brussels.
- Amdahl, J. (2009), *TMR4205 Buckling and Ultimate Strength of Marine Structures Chapter 3: Buckling of*

- Stiffened Shells*, MTS-2009.05.18.
- Bergan, P.G. and Holand, I. (1979), “Nonlinear finite element analysis of concrete structures”, *J Comput. Method Appl. Mech. Eng.*, **17-18**, 443-467.
- Byklum, E., Steen, E. and Amdahl, J. (2004), “A semi-analytical model for global buckling and postbuckling analysis of stiffened panels”, *Thin-Walled Struct.*, **42**, 701-717.
- ECCS TC8 TWG 8.4 (2008), *Shells, Buckling of Steel Shells European Design Recommendations*, ECCS, 5th Edition.
- Fujikubo, M., Harada, M., Yao, T., Khedmati, M.R. and Yanagihara, D. (2006), “Estimation of ultimate strength of continuous stiffened panel under combined transverse thrust and lateral pressure Part 2: Continuous stiffened panel”, *Marine Struct.*, **18**, 411-427.
- Khedmati, M.R., Zareei, M.R. and Rigo, P. (2009), “Sensitivity analysis on the elastic buckling and ultimate strength of continuous stiffened aluminium shells under combined in-plane compression and lateral pressure”, *Thin-Walled Struct.*, **47**, 1232-1245.
- Mittelstedt, C. (2007), “Closed-form analysis of the buckling loads of uniaxially loaded blade-stringer-stiffened composite shells considering periodic boundary conditions”, *Thin-Walled Struct.*, **45**, 371-382.
- Mittelstedt, C. (2009), “Explicit local buckling analysis of stiffened composite shells accounting for periodic boundary conditions and stiffener-shell interaction”, *Compos. Struct.*, **91**, 249-265.
- MSC Marc (2011), “*MSC Marc, Volume A: Theory and user information*”, MSC Software Corporation, USA.
- Naaman, A.E. (2000), *Ferrocement and Laminated Cementitious Composites*, Techno Press 3000., Ann Arbor, Michigan, USA.
- Paik, J.K., Kim, B.J. and Seo, J.K. (2008), “Methods for ultimate limit state assessment of ships and ship-shaped offshore structures: Part II stiffened panels”, *Ocean Eng.*, **35**, 271-280.
- Paik, J.K. and Seo, J.K. (2009), “Nonlinear finite element method models for ultimate strength analysis of steel stiffened-shell structures under combined biaxial compression and Lateral pressure actions—PartII: Stiffened panels”, *Thin-Walled Struct.*, **47**, 998-1007.
- Stamatelos, D.G., Labeas, G.N. and Tserpes, K.I. (2011), “Analytical calculation of local buckling and post-buckling behavior of isotropic and orthotropic stiffened panels”, *Thin-Walled Struct.*, **49**, 422-430.
- Tvergaard V. (1973), “Imperfection-Sensitivity of a wide integrally stiffened panel under compression”, *Int. J. Solid Structures*, **9**, 117-192,
- Ueda, Y., Rashed, S.M.H. and Paik J.K. (1995), “Buckling and ultimate strength in shells and stiffened panels under combined in plane biaxial and shearing forces”, *Marine Struct.*, **8**., 1-36.
- Ventsel, E. and Krauthammer, Th. (2001), *Thin Shells and Shells Theory, Analysis, and Applications*, Marcel Dekker INC., New York Basel.